Journal of Alloys and Compounds 615 (2014) S183–S187

Contents lists available at ScienceDirect

Journal of Alloys and Compounds

journal homepage: www.elsevier.com/locate/jalcom

Grain boundary wetting and premelting in the Cu–Co alloys

B.B. Straumal [a,b,c,d,*], A. Korneva [e], O. Kogtenkova [a], L. Kurmanaeva [f], P. Zięba [e], A. Wierzbicka-Miernik [e], S.N. Zhevnenko [d], B. Baretzky [b]

[a] Institute of Solid State Physics, Russian Academy of Sciences, Chernogolovka, Moscow District 142432, Russia
[b] Karlsruher Institut für Technologie, Institut für Nanotechnologie, Hermann-von-Helmholtz-Platz 1, 76344 Eggenstein-Leopoldshafen, Germany
[c] Moscow Institute of Physics and Technology (State University), Institutskii per. 9, 141700 Dolgoprudny, Russia
[d] Laboratory of Hybrid Nanostructured Materials and Department of Physical Chemistry, National University of Science and Technology "MISIS", 4 Leninsky pr., Moscow 119049, Russia
[e] Institute of Metallurgy and Materials Science, Polish Academy of Sciences, Reymonta St. 25, 30-059 Cracow, Poland
[f] Department of Chemical Engineering & Materials Science, University of California, One Shields Avenue, Davis, CA 95616, USA

ARTICLE INFO

Article history:
Available online 31 January 2014

Keywords:
Cu–Co alloys
Severe plastic deformation
High-pressure torsion
Grain boundaries
Wetting transition
Differential scanning calorimetry

ABSTRACT

The complete and incomplete wetting of Cu/Cu grain boundaries (GBs) by the Co-containing melt has been observed. The GB wetting in a peritectic system, where the GB wetting layer is depleted by a second component and not enriched like in the conventional cases, has been observed for the first time. The submicrograined structure in Cu–2.2 wt.% Co and Cu–4.9 wt.% Co alloys has been produced by the high pressure torsion. The melting process of both HPT-treated alloys was studied by the differential scanning calorimetry (DSC). The DSC melting curves were very asymmetric and have been deconvoluted into 2 and 4 different components, respectively. The positions of onsets and minima of high-temperature component peaks for both alloys correspond well with respective liquidus and solidus temperatures in the Cu–Co bulk phase diagram. The low-temperature component peaks were interpreted as GB premelting. The respective GB solidus line was constructed. The step-wise viscosity change of Cu–Co solid solutions was previously observed below the bulk solidus line. The viscosity changes 40–50 °C below the GB solidus line observed in this work. This difference can be explained by the difference in the GB character distribution or (alternatively) by the premelting in dislocations cores.

© 2014 Elsevier B.V. All rights reserved.

1. Introduction

Cu–Co is a well-known peritectic system [1,2], which has attracted considerable interest due to its magnetic properties (giant magnetoresistance [3]) and its application as catalyst in the synthesis of higher alcohols [4]. Therefore, the Cu–Co phase diagram has been recently extensively studied and reconsidered [5,6 and references therein]. The high positive mixing enthalpy leads not only to the interesting phenomena connected with metastable miscibility gap in the range of the undercooled melt [7,8 and references therein]. In the systems with positive mixing enthalpy the so-called grain boundary (GB) phase transformations; in particular GB wetting transitions can take place. In the Co-rich alloys (i.e. close to the eutectic temperature) such phenomena have been observed recently [9]. However, the GB wetting transitions have never been studied before in peritectic systems. From this point of view the Cu-rich Co–Cu alloys are very attractive and promising.

The GB phase transformations can drastically modify the properties of polycrystals [10,11]. Most important GB phase transformation is the transition from incomplete to complete wetting of a GB by a second phase. The wetting phase can be either liquid or solid. In case of incomplete wetting the contact angle between second phase and GB is non-zero $\theta > 0°$, and the wetting phase forms the lenticular particles separated by the "dry" GB portions. It is because the enthalpy of a GB unit area σ_{GB} is lower than that of two interphase boundaries σ_{IB}, namely $\sigma_{GB} < 2\sigma_{IB}$. In case of complete wetting $\sigma_{GB} > 2\sigma_{IB}$, $\theta = 0°$, and a layer of wetting phase completely substitutes a GB. The transition from incomplete to complete wetting of a GB by a liquid phase (melt) at a certain temperature T_w is described by a horizontal tie-line in the two-phase "solid solution + liquid" area of a bulk phase diagram [12,13]. Such tie-line connects the points at solidus and liquidus lines at T_w. According to simple thermodynamic calculations, this tie-lie cannot finish in its intersection with solidus line at T_w but has to continue in the one-phase "solid solution" area of a bulk phase diagram as a GB solidus line (or solvus line, if the second phase wetting the GB is solid) [14,15].

* Corresponding author at: Institute of Solid State Physics, Russian Academy of Sciences, Chernogolovka, Moscow District 142432, Russia. Tel.: +7 49652 23800, mobile: +7 916 6768673; fax: +7 499 2382326.

E-mail addresses: straumal@issp.ac.ru, straumal@mf.mpg.de (B.B. Straumal).

http://dx.doi.org/10.1016/j.jallcom.2014.01.156
0925-8388/© 2014 Elsevier B.V. All rights reserved.

By the intersection of the GB solidus or solvus lines the sudden change of GB properties can occur. In particular, the diffusivity drastically increases in the liquid-like GB layer [11,16], GB mobility becomes one order of magnitude higher [17], the multilayer segregation films form [18,19]. The first (temperature) derivative of GB energy breaks at the GB solidus line. It means that the prewetting/premelting is the phase transition of first order [19]. The measurements on the Cu–Bi samples showed that the electrical conductivity abruptly increased when the network of Bi-rich layers isolating the copper grains one from another had broken [18]. The extreme superplasticity of ultra-fine-grained Al–Zn–Mg alloys (with elongation to failure up to 2500%) in the narrow temperature interval just below the bulk solidus [20–25] is also driven by the formation of a liquid-like GB film [26,27] as a result GB wetting phase transition. The thin layers of the liquid-like Ni-rich phase were recently observed in the W–Ni system [14,28]. Such liquid-like GB layers phase appear because of the complete wetting of GBs in W and Mo by the liquid phase with lower melting point containing Ni, Co, Fe or Cu [29]. Thus, the GB solidus or solvus lines appear in the solid solution area of a bulk phase diagram if the melt of the second solid phase can completely wet the GBs in the respective two-phase areas of the same bulk phase diagram [11,13,26–30]. The second phase wetting GB in a first phase can be not only liquid but also solid [31].

Recently the creep behaviour of polycrystalline copper-based solid solutions and their surface tension has been studied under the solidus line of Cu–Co phase diagram [32,33]. The activation enthalpy for creep of pure copper was close to that of copper bulk self-diffusion. The activation enthalpy of creep of Cu–Co solid solutions was always lower than that of pure copper. Moreover, the experimental points for viscosity of Cu–Co solid solutions in Arrhenius coordinates can be approximated by the two straight lines with a break at a certain temperature. Such unusual creep behaviour of Cu–Co solid solutions has been explained by the change in grain boundary (GB) properties in studied coarse-grained polycrystals [32].

The goal of the present work is to prove the hypothesis that the abrupt increase of viscosity happens due to the intersection of GB solidus line in the Cu–Co phase diagram. First, we checked whether the Cu–Co melt can completely wet the GBs in Cu-based solid solution. Second, we investigated the melting heat release in the temperature interval close to the solidus line in Cu–Co alloys using the differential scanning calorimetry (DSC). The heat effects of the GB wetting and premelting phase transformations has been successfully observed previously in the Al-based alloys [34]. In order to increase possible input of GB wetting and premelting phenomena in DSC curves we applied the severe plastic deformation (SPD) to the studied Cu–Co alloys. SPD is known as a very powerful method of grain refinement and increase of the GB area in the unit volume [35,36].

2. Experimental

The Cu–Co alloys with 2.2 and 4.9 wt.% Co in form of 10 mm diameter rods were prepared by a vacuum induction melting and casting from the high-purity 5 N Cu and Co. The 0.6 mm thick as-cast disks of studied alloys obtained after grinding, sawing and chemical etching were subjected to high pressure torsion (HPT) at room temperature under the pressure of 6 GPa in a Bridgman anvil type unit (5 torsions, 1 rpm). Samples for structural and calorimetric investigations were cut from the HPT-processed discs at a distance of 3 mm from the sample centre. For the investigations of GB wetting behaviour a set of the as-cast Cu–2.2 wt.% Co alloys samples was sealed into evacuated silica ampoules with a residual pressure of approximately 4×10^{-4} Pa at room temperature. Samples were annealed at temperatures between 1085 and 1100 °C for 30 min, and then quenched in water. The accuracy of the annealing temperature was ±1 °C. The HPT-treated samples were studied with use of the DSC 404 F1Pegasus, Netzsch in argon atmosphere and of TA Instruments calorimeter (model Q1000) in dry helium, at cooling and heating rates of 10 °C/min. In order to record the DSC curves, the samples were heated from 50 to 1300 °C. The complicated DSC peaks were first approximated with polynoms and than deconvoluted using the Netzsch Peak Separation program version 2008.05. For each deconvoluted peak the temperature of onset T_{onset}, minimum T_{min} and enset T_{endset} was determined (Tables 1 and 2). According to the standard procedure, the temperature T_{onset} and T_{endset} of the peak was marked as the point of intersection of the tangent drawn through the inflection point of the curve with the extrapolated baseline. For the metallographic investigations the samples were ground by SiC grinding paper, polished with 6, 3, and 1 μm diamond pastes and etched for 5–10 s in 1:1 solution of H_2O and HNO_3. Light microscopy (LM) was performed on a Zeiss Axiophot microscope. Scanning electron microscopy (SEM) investigations were carried out on a Philips XL30 scanning microscope equipped with a LINK ISIS energy-dispersive spectrometer produced by Oxford Instruments. X-ray diffraction (XRD) data were obtained on a Siemens diffractometer (Co Kα radiation). Grain size was estimated by the XRD line broadening using the Scherrer formula [37].

3. Results and discussion

In Fig. 1a the SEM micrograph of Cu–2.2 wt.% Co sample annealed at 1094 °C is shown. According to the bulk phase diagram [5,6,38], the solidus and liquidus temperature for this alloy are 1091 and 1097 °C, respectively. Almost all GBs in Fig. 1a are completely wetted ($\theta = 0°$). In Fig. 1b the Co concentration profile across completely wetted Cu GB is shown. In this plot the position of Cu GB corresponds to the minimum of Co content. It is because the peritectic transformation takes place in the Cu-rich alloys, and melted wetting phase contains less Co than the Cu-based solid solution. Therefore, the complete and incomplete GB wetting in the peritectic system has been observed for the first time, where the GB wetting layer is depleted by a second component and not enriched like in the conventional cases [11–13,26,27,34].

The microstructure of as-cast alloys contains the supersaturated Cu-based solid solution and Co precipitates [15]. The size of (Cu) grains in both alloys is between 15 and 22 μm. A certain tendency to the faceting of Co/Cu interphase boundaries was present [19,39]. After HPT the grain size drastically decreases to about 100 nm for the Cu-grains and 30 nm for the Co-precipitates. Cu grains are almost equiaxial; the Co-particles are uniformly distributed among Cu grains. HPT leads also to the partial dissolution of Co precipitates in Cu-based matrix. The rate of this dissolution was very high (about a half of existed Co precipitates dissolved in 5 min of HPT treatment), despite of the known fact that the application of high pressure, even without deformation always decreases the diffusivity and grain boundary mobility [40,41]. The heating of HPT-treated alloys in the DCS apparatus at a rate of 10 °C/min leads to a certain grain growth. Below bulk solidus line the grain size was about 10–30 μm.

In Fig. 2a the temperature dependence of heat flow (DSC curve) is shown for the HPT-treated Cu–2.2 wt.% Co alloy heated from 50 to 1300 °C at a rate of 10 °C/min. Only the high-temperature part between 1066 and 1116 °C is shown in Fig. 2a. The integral heat effect of melting (melting enthalpy) was about 104% of that for pure copper (208.7 J/g [42,43]). In Fig. 2b the temperature dependence of heat flow (DSC curve) is shown for the HPT-treated Cu–4.9 wt.% Co alloys heated from 50 to 1300 °C at a rate of 10 °C/min. Only the high-temperature part between 1078 and 1122 °C is shown in Fig. 2b. The integral heat effect of melting (melting enthalpy) was about 98.4% of that for pure copper.

Both DSC curves shown in Fig. 2 have complicated form, with overlapping peaks. These DSC peaks were first approximated with polynoms (thin line) and than deconvoluted using the Peak

Table 1
Results of deconvolution of melting curve for the DSC melting curve for the Cu–2.2 wt.% Co alloy (Fig. 2a).

Curve in Fig. 2	Onset (°C)	Minimum (°C)	Endset (°C)	Symbol in Fig. 3
2 (dotted)	1077.1	1082.3	1094.9	Open circles
1 (dashed)	1085.8	1098.0	1103.4	Filled diamonds

Table 2
Results of deconvolution of melting curve for the DSC melting curve for the Cu–4.9 wt.% Co alloy (e.g. Fig. 2a).

Curve in Fig. 2	Onset (°C)	Minimum (°C)	Endset (°C)	Symbol in Fig. 3
4 (Dashed)	1065.7	1068.6	1073.6	Open circles
2 (Dotted)	1085.1	1088.2	1092.3	Open down-triangles
3 (Dot-dashed)	1072.7	1095.9	1111.9	Open up-triangles
1 (Dot-dot-dashed)	1098.7	1108.2	1113.2	Filled diamonds

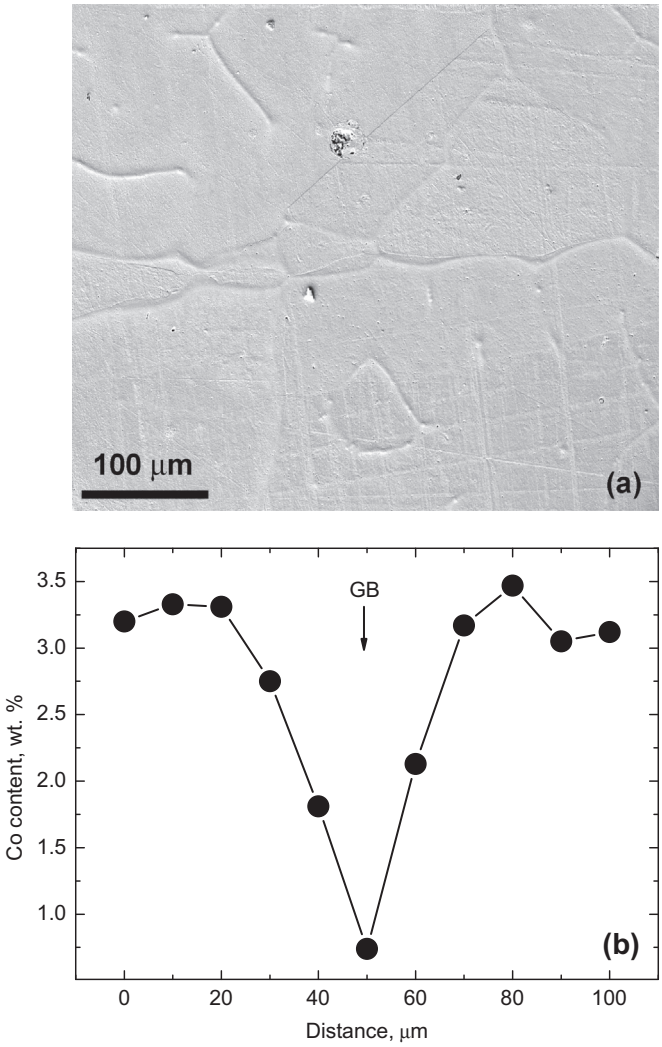

Fig. 1. (a) SEM micrograph of Cu–2.2 wt.% Co sample annealed at 1094 °C. (b) Co concentration profile across completely wetted Cu GB.

Separation program version 2008.05. The DSC curve for the Cu–2.2 wt.% Co alloy contains two peaks (Table 1) and the DSC curve for the Cu–4.9 wt.% Co alloy was deconvoluted into four peaks (Table 2). We used the standard approach for quantification of the DSC curves [44] (these procedures are also included in the quantification software of modern DSC equipment). According to this approach, for melting of an alloy between the solidus and liquidus temperatures, the onset point corresponds to the start of melting and position of a deep minimum corresponds to the end of melting, i.e. to the liquidus temperature. The onset temperature of the peak was determined as the point of intersection of the tangent drawn through the inflection point of the curve with the extrapolated baseline. The measured minimum positions (peak 2 in Fig. 2a for the Cu–2.2 wt.% Co alloy and peak 4 in Fig. 2b for the Cu–4.9 wt.% Co alloy for both samples correspond well to the literature data for the liquidus temperatures in the Cu–Co system (filled diamonds in Fig. 3) [5,6,38]. The onset positions for the peak 2 for the Cu–2.2 wt.% Co alloy and peak 4 for the Cu–4.9 wt.% Co alloy correspond well to the literature data for the solidus temperatures in the Cu–Co system (filled diamonds in Fig. 3) [5,6,38]. However, the DSC peaks consist of several overlapping peaks. The peak 2 in the Cu–2.2 wt.% Co alloy (Fig. 2a, Table 1) and peaks 2–4 in the Cu–4.9 wt.% Co alloy (Fig. 2b, Table 2) are positioned below the solidus line in the Cu–Co system (Fig. 3).

In Fig. 3 the Cu-rich part of the Cu–Co phase diagram is shown. Thick lines denote the bulk phase transitions [5,6,38]. Thin horizontal line in the L+(Cu) area is the tie-line of GB wetting phase transition. It marks the temperature $T_{W50\%}$ where 50% of (Cu) GBs are completely wetted by the liquid phase L. Filled diamonds denote the positions of the highest onsets and minima in the DSC curves (curve 1) for both studied Cu–Co alloys (Fig. 2, Tables 1 and 2). They coincide with solidus and liquidus lines of the Cu–Co phase diagram [5,6,38]. Open circles denote the positions of the lowest onsets and minima in the DSC curves for both studied Cu–Co alloys (curve 2 in Fig. 2a, Table 1 and curve 4 in Fig. 2b, Table 2). We suppose that the heat effect below bulk solidus line is due to the formation of thin liquid like layer in GBs. GBs start to melt at temperatures below the melting in the bulk. The usual condition for the GB premelting is the existence of complete GB wetting in the (Cu)+L area of the Cu–Co phase diagram. It has been observed indeed in our samples (Fig. 1). Therefore, we can draw the GB solidus line (dashed line in Fig. 3) through the onsets of peak 1 (Tables 1 and 2) in both alloys (open circles in Fig. 3). It is extremely complicated to directly observe the thin liquid like layer in GBs between GB solidus and bulk solidus line. First of all, it is because the direct in situ structural TEM or X-rays diffraction observations are very hard to convey due to the high temperature. If the samples are quenched, it is sometimes possible to observe the transformed thin GB layers by TEM or Auger electron spectroscopy [14,26,28]. Therefore, the value of indirect high-temperature experiments is so high. They can demonstrate that GBs between GB solidus and bulk solidus possess different energy [19], high mobility [17], high ductility [20–25] or brittleness [36], high diffusivity [16], different electrical resistivity [18]. DSC shows that GBs start to melt below bulk solidus line and this effect becomes more pronounced with decreasing grain size [34]. GB liquid-like layer in a one-phase area of a bulk phase diagram appears and disappears together with complete GB wetting in a two-phase S + L area of a bulk phase diagram [36].

In any case, the obtained results give the strong evidence that the liquid-like GB layers exist also in the Cu–Co system. It looks very promising for the future experiments especially because the GB premelting layers should be depleted by the second component (similar to the wetting liquid) and not enriched like in all studied eutectic and eutectoid systems [11–13,18,27–29,31,34].

Open up- and down-triangles in Fig. 3 correspond to the onset and a minimum in the DSC curves 3 and 2 (Table 2) for the Cu–4.9 wt.% Co alloy. They are intermediate between GB and bulk solidus lines. Recently we already observed the asymmetric shape of the melting curve measured in Al–Mg alloys [34]. The difference in the shape of the melting curve for the two studied alloys was explained by the different temperature dependence of the fraction

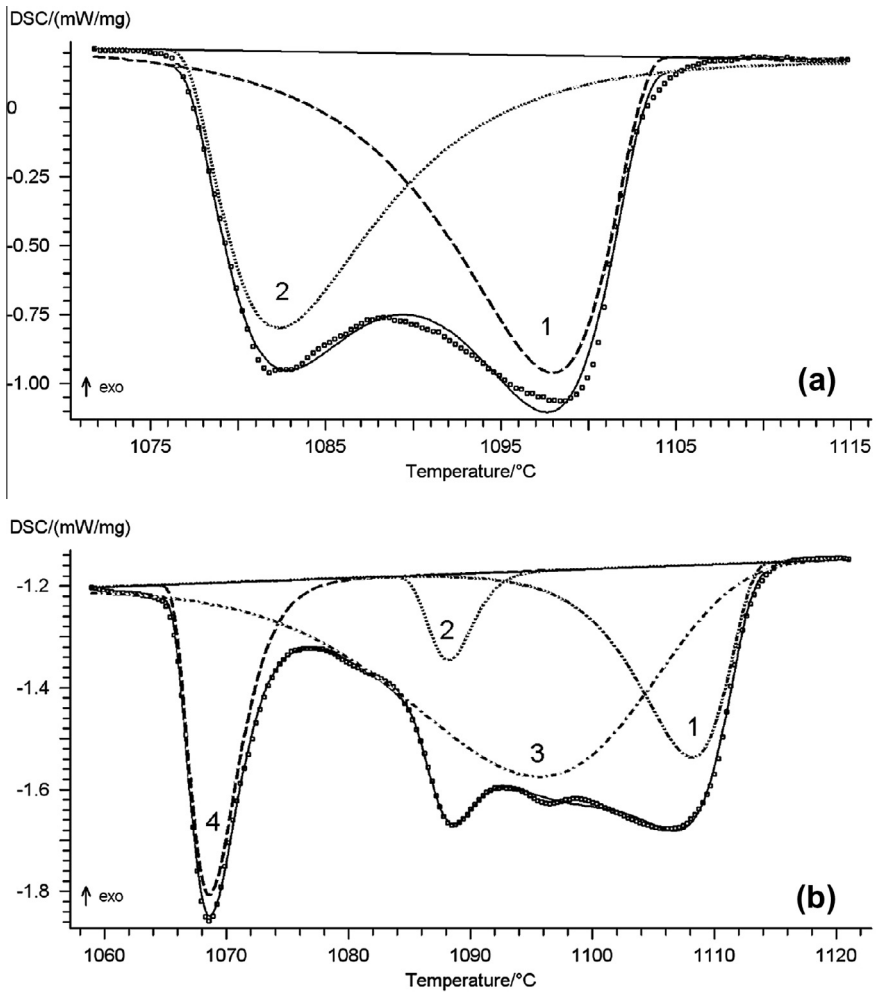

Fig. 2. Temperature dependence of heat flow (DSC curve) for the (a) Cu–2.2 wt.% Co and (b) Cu–4.9 wt.% Co alloys. The peaks are deconvoluted using the Peak Separation program version 2008.05. The square points – experimental data; solid line – the sum of separated peaks; dotted and dashed lines – separated peaks.

of completely wetted grain boundaries. Similar to that case, we suggest that the GB premelting transition takes place at different temperatures at GBs with different character and different energies. This is effect reflects itself in several minima between GB and bulk solidus lines and is resolved in the melting curve (Fig. 2b).

The obtained DSC curves have a quite complicated shape. Most probably, another decomposition procedure would result in other array of offset, minimum and endset temperatures. It rather clear that the polycrystals with different GB character distribution would have different DSC curves. It is because the GB solidus line shown in Fig. 3 is the envelope (or resultant) of numerous solidus lines for individual GBs in a polycrystal. However, in any case, the DSC curves undoubtedly show that melting in fine-grained Cu–Co polycrystals starts well below the bulk solidus.

Wu and Perepezko recently showed that the determination of liquidus by thermal analysis in multicomponent alloys is not so straightforward as in pure elements [45]. For example the minima in DSC curves in multicomponent alloys do not correspond to the end of melting. We can see it in our curves as well (Fig. 2). Namely, only the minimum of peak 1 in both alloys coincides more or less with bulk liquidus known from the literature (filled diamonds in Fig. 3). Minimum of peaks 2, 3 and 4 lies below the bulk liquidus line (open symbols in Fig. 3). However, for us not the end of melting but the start of meting is important (it happens 10–30 °C below the bulk solidus line).

Open squares in Fig. 3 denote the positions of the breaks in temperature dependences of the viscosity of Cu–Co solid solutions [32]. We drove a dotted line (a guide for the eyes) through these points. They lie about 40–50 °C below the GB solidus (dashed line in Fig. 3) obtained using the DSC data from Fig. 2. It means that the abrupt change in the creep properties of Cu–Co polycrystals do not exactly coincide with the GB solidus line obtained using the DSC curves. The reasons for this discrepancy have to be carefully investigated in the future. For example, it is known that the one-dimensional tubes of wetting and/or prewetting phase can also form along dislocations [46]. However, the dislocations input into creep at high temperatures (close to solidus line) and very low stresses cannot control the creep rate. More realistic would be to suppose that the shift of GB solidus to lower temperatures can be explained by the shift of GB energy to the higher values. It is because during the creep deformation the GBs permanently serve as a sink of lattice vacancies diffusing from the source (free surface). The increased vacancies concentration makes GBs non-equilibrium, increases the GB energy, and decreases the premelting temperature.

Another reason can be the difference in the GB character distribution. In other words, the spectrum of GB misorientations and inclinations is different in samples after HPT with subsequent heating and in samples after high-temperature creep. The resulting mean GB energy is than lower in polycrystals after HPT. For example it is very well known that Cu and Cu-based alloys contain a very high (sometimes >50%) percentage of twin GBs ($\Sigma 3$) and other low-energy near coincidence boundaries (like $\Sigma 9$, $\Sigma 5$, etc.) [47]. On the other hand, it has been recently demonstrated that not only

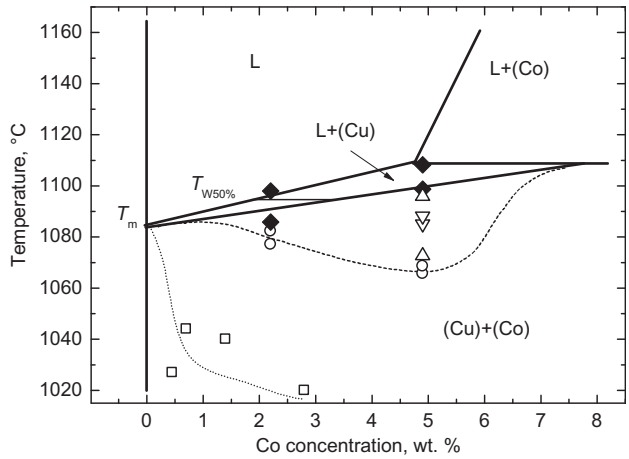

Fig. 3. Cu-rich part of the Cu–Co phase diagram. Thick lines denote the bulk phase transitions [5,6,38]. Thin horizontal line in the L+(Cu) area is the tie-line of GB wetting phase transition. It marks the temperature $T_{W50\%}$ where 50% of (Cu) GBs are completely wetted by the liquid phase L. Filled diamonds denote the positions of the highest onsets and minima in the DSC curves (curve 1) for both studied Cu–Co alloys (Fig. 2, Tables 1 and 2). They coincide with solidus and liquidus lines of the Cu–Co phase diagram [5,6,38]. Open circles denote the positions of the lowest onsets and minima in the DSC curves for both studied Cu–Co alloys (curve 2 in Fig. 2a, Table 1 and curve 4 in Fig. 2b, Table 2). They correspond to the position of GB solidus line (dashed line). Open up- and down-triangles correspond to the onsets and minima in the DSC curves 3 and 2 (Table 2) for the Cu–4.9 wt.% Co alloy. Open squares denote the positions of the breaks in temperature dependences of the viscosity of Cu–Co solid solutions [32]. Dotted line is the guide for the eyes and denotes the possible position of another GB solidus reflecting itself in the creep properties of Cu–Co polycrystals.

GBs with low Σ but generally all tilt GBs belong to the top 10% of the overall GB energetic spectrum in a conventional polycrystal [48]. In any case, the GB character distribution close to the bulk solidus line should be carefully compared in the future (for example using electron back-scattering diffraction – EBSD) in samples after slow plastic deformation (creep) and after severe plastic deformation.

To conclude, we observed that the melt can completely wet the grain boundaries in the peritectic Cu–Co alloys. Moreover, this GB wetting layer is depleted by a second component and not enriched like in conventional eutectic systems. The position of DSC peaks showed that melting of ultrafine-grained Cu–Co alloys starts 10–30 °C below the solidus line. The thermal effects of melting below bulk solidus line are explained by the GB premelting and permitted to construct the GB solidus line. The step-wise change of creep parameters happened 40–50 °C below the observed GB solidus line. It can be explained by the difference in the GB character distribution or (alternatively) by the premelting in dislocations cores.

Acknowledgements

Authors thank the Russian Foundation for Basic Research (Contracts 12-03-00894, 13-08-90422 and 14-08-00972), the Russian Federal Ministry for Education and Science (Grant 14.A12.31.0001), EraNet.Rus programme (Grant STProjects-219), Program of bilateral cooperation between Russian and Polish Academies of sciences, Russian Federal Ministry of Education and Science, Karlsruhe Nano Micro Facility and Polish National Science Centre (Grant UMO-2011/01/M/ST8/07822) for the financial support.

References

[1] T. Nishizawa, K. Ishida, Bull. Alloys Phase Diagrams 5 (1984) 161–165.
[2] Y. Nakagawa, Acta Metall. 6 (1958) 704–711.
[3] G. Binasch, P. Gruenberg, F. Saurenbach, W. Zinn, Phys. Rev. B 39 (1989) 4828–4830.
[4] J.P. Hindermann, G.J. Hutchings, A. Kiennemann, Catal. Rev. – Sci. Eng. 35 (1993) 1–127.
[5] M.A. Turchanin, P.G. Agraval, Powder Metall. Met. Ceram. 46 (2007) 77–89.
[6] M. Palumbo, S. Curiotto, L. Battezzati, Comput. Coupling Phase Diagrams Thermochem. 30 (2006) 171–178.
[7] B. Schwarz, N. Mattern, O. Shuleshova, J. Eckert, Intermetallics 32 (2013) 250–258.
[8] S. Curiotto, R. Greco, N.H. Pryds, E. Johnson, L. Battezzati, Fluid Phase Equilib. 256 (2007) 132–136.
[9] S. Curiotto, D. Chatain, Scripta Mater. 60 (2009) 40–43.
[10] Th.R. Bieler, R. Barabash, D. Spearot, J. Luo, S. Dillon, Metall. Mater. Trans. A 43 (2012) 3515–3516.
[11] B. Straumal, W. Gust, D. Molodov, Interface Sci. 3 (1995) 127–132.
[12] B.B. Straumal, W. Gust, Mater. Sci. Forum 207 (1996) 59–68.
[13] B.B. Straumal, W. Gust, T. Watanabe, Mater. Sci. Forum 294 (1999) 411–414.
[14] V.K. Gupta, D.H. Yoon, H.M. Meyer, J. Luo, Acta Mater. 55 (2007) 3131–3142.
[15] B.B. Straumal, S.G. Protasova, A.A. Mazilkin, B. Baretzky, D. Goll, D.V. Gunderov, R.Z. Valiev, Philos. Mag. Lett. 89 (2009) 649–654.
[16] B.B. Straumal, O.I. Noskovich, V.N. Semenov, L.S. Shvindlerman, W. Gust, B. Predel, Acta Metall. Mater. 40 (1992) 795–801.
[17] D.A. Molodov, U. Czubayko, G. Gottstein, L.S. Shvindlerman, B.B. Straumal, W. Gust, Philos. Mag. Lett. 72 (1995) 361–368.
[18] B. Straumal, N.E. Sluchanko, W. Gust, Diffus. Defect Data, Pt. A 188–190 (2001) 185–194.
[19] J. Schölhammer, B. Baretzky, W. Gust, E. Mittemeijer, B. Straumal, Interface Sci. 9 (2001) 43–53.
[20] K. Higashi, T.G. Nieh, M. Mabuchi, J. Wadsworth, Scr. Metall. Mater. 32 (1995) 1079–1084.
[21] Y. Takayama, T. Tozawa, H. Kato, Acta Mater. 47 (1999) 1263–1270.
[22] M. Mabuchi, K. Higashi, Y. Okada, S. Tanimura, T. Imai, K. Kubo, Scr. Metall. 25 (1991) 2003–2006.
[23] K. Higashi, Y. Okada, T. Mukai, S. Tanimura, Scr. Metall. 25 (1991) 2053–2057.
[24] H. Iwasaki, T. Mori, M. Mabuchi, K. Higashi, Acta Mater. 46 (1998) 6351–6360.
[25] B. Baudelet, M.C. Dang, F. Bordeaux, Scr. Metall. Mater. 26 (1992) 573–578.
[26] B.B. Straumal, A.A. Mazilkin, O.A. Kogtenkova, S.G. Protasova, B. Baretzky, Philos. Mag. Lett. 87 (2007) 423–430.
[27] B. Straumal, O. Kogtenkova, S. Protasova, A. Mazilkin, P. Zieba, T. Czeppe, J. Wojewoda-Budka, M. Faryna, Mater. Sci. Eng., A 495 (2008) 126–131.
[28] J. Luo, V.K. Gupta, D.H. Yoon, H.M. Meyer, Appl. Phys. Lett. 87 (2005) 231902.
[29] E. Rabkin, D. Weygand, B. Straumal, V. Semenov, W. Gust, Y. Bréchet, Philos. Mag. Lett. 73 (1996) 187–193.
[30] V.N. Semenov, B.B. Straumal, V.G. Glebovsky, W. Gust, J. Cryst. Growth 151 (1995) 180–186.
[31] G.A. López, E.J. Mittemeijer, B.B. Straumal, Acta Mater. 52 (2004) 4537–4545.
[32] S.N. Zhevnenko, E.I. Gershman, J. Alloys Comp. 536S (2012) S554–S558.
[33] S.N. Zhevnenko, Metall. Mater. Trans. A 44 (2013) 2533–2538.
[34] O.A. Kogtenkova, S.G. Protasova, A.A. Mazilkin, B.B. Straumal, P. Zięba, T. Czeppe, B. Baretzky, J. Mater. Sci. 47 (2012) 8367–8371.
[35] R.Z. Valiev, R.K. Islamgaliev, I.V. Alexandrov, Prog. Mater. Sci. 45 (2000) 103–189.
[36] B. Baretzky, M.D. Baró, G.P. Grabovetskaya, J. Gubicza, M.B. Ivanov, Yu.R. Kolobov, T.G. Langdon, J. Lendvai, A.G. Lipnitskii, A.A. Mazilkin, A.A. Nazarov, J. Nogués, I.A. Ovidko, S.G. Protasova, G.I. Raab, Á. Révész, N.V. Skiba, J. Sort, M.J. Starink, B.B. Straumal, S. Suriñach, T. Ungár, A.P. Zhilyaev, Rev. Adv. Mater. Sci. 9 (2005) 45–108.
[37] T. Ungar, A. Borbely, Appl. Phys. Lett. 69 (1996) 3173–3175.
[38] T.B. Massalski (Ed.), Binary Alloy Phase Diagrams, ASM International, Materials Park, OH, 1990.
[39] B.B. Straumal, S.A. Polyakov, E. Bischoff, W. Gust, E.J. Mittemeijer, Interface Sci. 9 (2001) 287–292.
[40] D.A. Molodov, B.B. Straumal, L.S. Shvindlerman, Scr. Metall. 18 (1984) 207–211.
[41] B.B. Straumal, L.M. Klinger, L.S. Shvindlerman, Scr. Metall. 17 (1983) 275–279.
[42] R. Hultgren et al., Selected Values of Thermodynamic Properties of the Elements, American Society for Metals, Metals Park, OH, 1973.
[43] C. Cagran, B. Wilthan, G. Pottlacher, Thermochim. Acta 445 (2006) 104–110.
[44] J.A. Dean, The Analytical Chemistry Handbook, McGraw Hill, New York, 1995 (Standards ASTM D 3417, ASTM D 3418, ASTM E 1356, ISO 11357).
[45] R.I. Wu, J.H. Perepezko, Metall. Mater. Trans. A 31 (2000) 497–501.
[46] L.-S. Chang, W. Lojkowski, B. Straumal, E. Rabkin, W. Gust, Acta Mater. 55 (2007) 335–343.
[47] X. Sauvage, G. Wilde, S. Divinsky, Z. Horita, R.Z. Valiev, Mater. Sci. Eng., A 540 (2012) 1–12.
[48] B.B. Straumal, P.V. Protsenko, A.B. Straumal, A.O. Rodin, Yu.O. Kucheev, A.M. Gusak, V.A. Murashov, JETP Lett. 96 (2012) 582–587.